X-ray Absorption Spectroscopic Studies on Nickel Catalysts for Epoxidation*

Martin C. Feiters,[a*] Gerald A. Metselaar,[a] Bastienne B. Wentzel,[a]
Roeland J. M. Nolte,[a] Serge Nikitenko,[b] David C. Sherrington,[c]
Y. Joly,[d] Grigory Yu. Smolentsev,[e] Antonina N. Kravtsova,[e] Alexander V. Soldatov[e]

a) Department of Organic Chemistry, Institute for Molecules and Materials, Radboud University Nijmegen, 1 Toernooiveld, 6525 ED Nijmegen, NL
Email: M.Feiters@science.ru.nl, phone +.31.24.3652016, fax +.31.24.3652929
b) DUBBLE CRG/ESRF (FWO), c/o ESRF BP 220, F-38043 Grenoble Cedex, France
c) Department of Pure & Applied Chemistry, University of Strathclyde, 295 Cathedral St., Glasgow G1 1XL, UK
d) Laboratoire de Cristallographie, Centre National de la Recherche Scientifique, Associé à l'Université Joseph Fourier, Boîte Postale 166, F-30842 Grenoble Cedex 9, France
e) Faculty of Physics, Rostov State University, Sorge 5, Rostov-na-Donu, 344090 Russia

*) Dedicated to Prof. David C. Sherrington on the occasion of his 60th birthday.

Abstract

We have studied epoxidation catalysts based on complexes of nickel with acac (acetylacetonate) ligands in the solid state, in solution and on a polymeric support by X-ray absorption spectroscopy. The EXAFS results show that the degree of association (monomer or trimer) of the Ni(acacR) complexes depends on the bulkiness of R. For R = H, trimers predominate both in the solid state and in solution, whereas for R = p-tBuBn, the monomers that are found in the solid state tend to associate to trimers in solution. The trimers are broken up by excess coreactant, i-butyraldehyde, which converts all Ni complexes to 6-coordinated species. The lower degree of association of the substituted Ni(acacR) complex accounts for its relatively high catalytic activity at low concentration. For the solid complexes, the EXAFS results, which provide 1-dimensional structural information, are complemented by XANES simulations defining the 3-dimensional structure around Ni. The benzimidazole and pyridine ligands of PBI and AMP-resin partially displace acac in the Ni ligand sphere upon grafting. For the rigid PBI this must result in vacancies in the Ni coordination sphere, which explains why this support gives an active catalyst whereas the AMP-resin does not.

Introduction

$Ni(acacR)_2$ complexes **1** show remarkable efficiency in the Mukaiyama epoxidation, a reaction (Scheme 1) where one oxygen atom of molecular oxygen is transferred to an alkene yielding an epoxide, while the other is accepted by the coreactant, i-butyraldehyde.[1] We have recently proposed a mechanism for this reaction in which an oxygen atom is transferred to the alkene by an acylperoxy radical; this radical arises from the reaction of molecular oxygen with an acyl radical, generated from aldehyde by the Ni complex in its Ni(III) form (Scheme 2).[2] At concentrations lower than 0.5 mM, complex **1b** (R = *p*-tBuBn) is more active than **1a** (R = H); access of reactants to the Ni ion is made more difficult by the bulky substituent, but on the other hand it is also expected to prevent assembly into an inactive trimer (Scheme 3, top part) as observed in the crystal structure[3,4] for **1a**. We have also investigated the effect of grafting $Ni(acac)_2$ **1a** on ligand containing polymer supports (Scheme 4).[5] Grafting onto PBI (polybenzimidazole)[6] resulted in an active catalyst, whereas grafting on AMP-resin (an aminomethylpyridine methacrylate-type resin)[7] did not.

- - - SCHEME 1, 2, 3, 4 - - -

We now report on a study of the metal environment in Ni-containing epoxidation catalysts in the solid state, in solution (using a specially developed solution cell)[8] and on polymeric supports by X-ray absorption spectroscopy.[9] The fine structure in X-ray absorption spectra is caused by X-ray induced electron diffraction which leads to single scattering events involving ligand atoms (EXAFS), as well as multiple scattering effects within (EXAFS, XANES) and between (XANES) ligand molecules.

The EXAFS (extended X-ray absorption fine structure) part of the X-ray absorption spectrum can be Fourier transformed to give a radial distribution of atoms around the central atom (Ni), and simulated to give type (Z, ± 1), number (N, ±1), and distance (R, ± 0.02 Å) of the surrounding atoms. The classical approach[9] is to simulate the shells of atoms in the Fourier transform one by one after Fourier filtering and back-transformation. In the present work, we have simulated the EXAFS with units representing whole ligand (acac, benzimidazole, and pyridine) moieties rather than shells of atoms, including the contributions of multiple scattering between the shells in the units in the programme EXCURVE,[10,11] and using reasonable interatomic distances within the ligands as restraints in the refinement.[12]

The XANES (X-ray absorption near edge structure) part of the X-ray absorption spectrum is sensitive to the valence and coordination geometry of the central atom, but also to angular and nearest neighbour effects.[13] The classical approach to interpret the XANES part of the spectrum is to make comparisons with a number of well-characterised model compounds, and data on a range of interesting Ni compounds have been collected.[14] In the present work we have simulated the XANES spectra on the basis of 3-dimensional models.

We demonstrate that the combination of EXAFS analysis followed by modeling of the nickel atom surrounding in Ni acac and the subatomic resolution provided by XANES spectroscopy is a very powerful approach for structural studies of Ni acac complexes. This technique allows XANES data to be calculated for the model structures constructed on the basis of EXAFS simulations, and to decide on the best structural model by comparison with the experimental XANES spectrum.

By comparing the EXAFS results for the epoxidation catalysts in the solid state, in solution, and on polymeric supports, the observed[2,5] differences in ractivity can be explained.

Experimental Section

Sample preparation and measurements. Ni(acacR)$_2$ complexes[1] and Ni-containing polymers[5] were obtained as described earlier, *i*-butyraldehyde was from Aldrich. Solid samples were diluted with boron nitride and measured in transmission mode, whereas solutions (5 mM in Ni) were measured in a specially developed solution cell[8] in fluorescence mode. A complete set of X-ray absorption spectra was recorded at room temperature and 77 K at the 'Anglo-Dutch' station 8.1[15] at the SRS (Synchrotron Radiation Source) of the CLRC Daresbury Laboratory, UK. More recently some samples were measured at the EXAFS station of DUBBLE/ESRF (BM 26) at room temperature.

EXAFS simulations. The Fourier-filtered (non-phaseshift corrected R range 0.8 – 6.0 Å) back-transformed EXAFS was simulated with EXCURVE version 9.272 using FEFF phaseshifts. The geometrical input for the simulations as grouped in 2-dimensional units of atoms (not including hydrogens) representing the possible ligand molecules. The shells of atoms in a certain units all had the same occupancy, and in the iterative refinement of the simulations, all interatomic distances, apart from the distance to the central Ni ion,

were restrained to lengths based on relevant crystallographic data. This so-called restrained refinement[12] implies that in the iterative refinement, the restrained parameters have freedom to move in a direction where they will lower the fit index, but also that a penalty will be added to the fit index depending on the deviation from the idealized value, the restraint.

The geometries and restraints of the units representing the bidentate and monodentate acac ligand[3,4,16] are shown in Scheme 5 along with the applied restraints. The imidazole[17] and pyridine[18] moieties were represented by ideal polygons, viz. a pentagon with the distances between the ring atoms restrained to 1.34 Å for imidazole, and a hexagon with a restrained distance of 1.37 Å for pyridine. In addition, equivalent atoms in the the bidentate acac, the pyridine, and the imidazole units were constrained in the refinement to have identical distances to Ni and Debye-Waller-type factors. The isobutyraldehyde ligand was represented by the coordinating carbonyl and the carbon directly attached to it, with the C=O and C-C distances restrained to 1.35 and 1.54 Å, respectively.

- - - SCHEME 5 - - -

XANES simulations. XANES spectroscopy has been well established as a technique that is more sensitive to angular and nearest neighbour effects than EXAFS spectroscopy. [13] Unfortunately, unlike EXAFS spectra, XANES spectra cannot be readily analyzed via Fourier transform methods, so that it has been difficult to extract detailed structural parameters from XANES and EXAFS has been used much more for structural analysis.

Recently, analysis of the spectroscopic features in XANES data has improved due to development of efficient codes for the calculation of x-ray absorption.[19-21] Multiple-scattering XANES calculations are more challenging than EXAFS calculations, since electron scattering is much stronger and a multiple-scattering regime for the photoelectron takes place at low energies, and hence XANES data are much more sensitive to details of the scattering potential and to the distribution of atoms around the photo-absorbing ion.[22] It can be necessary to use a more advanced theoretical approach, such as calculations of the molecular potential without the so-called "muffin-tin" approximation.[23]

We used the FDMNES package,[24] which runs within the real space cluster approach, and uses the finite difference method (FDM) to solve the Schrödinger equation. Its main advantage is the possibility to have a totally free potential shape, thus getting rid of the muffin-tin limitations. In addition, we make a Lorentzian energy-dependent convolution of the spectrum to account for the multielectronic and inelastic phenomena occurring in the absorption process. At the Fermi level, the Lorentzian width is due to both the interaction with the core hole and the monochromator resolution. For higher photoelectron energy, between 10 and 40 eV, the onset of plasmons collective interactions increase the Lorentzian width up to 6 eV.

Results and Discussion

EXAFS and XANES of solid Ni(acacR)$_2$ complexes.

In Figure 1 the spectra of Ni(acacR)$_2$ with R = H (**1a**) and R = *p*-tBuBn (**1b**) in the solid state are compared. Apparently, the introduction of the bulky substituent in **1b** has resulted in a complex with a significantly shorter Ni-ligand distance, which is in line with the expected change from a trimer, in which each Ni has octahedral 6-coordination, for **1a**, to a monomeric complex with square-planar 4-coordination for Ni in **1b**. The fact that the major peak in the Fourier transform at approx. 2 Å seems to be decreased in amplitude and is broadened appears at first sight to be inconsistent with an increase in coordination number. This broadening must be a result of the disorder, resulting in high values for the Debye-Waller-type factors, which is also a feature of the known crystal structures for **1a**. Following the original report on the trimeric structure of **1a**,[3] with Ni-O distances ranging from 1.89 to 2.27 Å (average 2.08 Å), the crystal structure was redetermined and refined to a lower R-value,[4] but still shows a spread in the Ni-O distances from 1.93 to 2.31 Å (average 2.06 Å). Close inspection of this most recent crystal structure revealed that each Ni ion in the trimer has 2 bidentate acac ligands with Ni-O distances ranging from 1.93 to 2.07 Å (average 2.00 Å), and that each Ni ion has longer contacts (2.08-2.31 Å, average 2.20 Å, relatively short for the central Ni) with one of the oxygens of the acac ligands that are bidentate ligands to one of the other Ni ions.

Preliminary simulations showed that the EXAFS for **1a** could be explained with bidentate acac units, or 2 bidentate acac units + 2 more remote O atoms per Ni, but also that this did not reproduce the spectrum entirely satisfactorily. The agreement between theory and experiment was not only assessed by the fit index for the EXAFS, but also by visual inspection of the EXAFS, the Fourier transform, and the imaginary part of the

Fourier transform. It can be recognized (Scheme 5) that both in the bidentate and monodentate acac ligand geometries, there are many scattering pathways where the angle Ni-close backscatterer-remote backscatterer is between 120 and 180 degrees; therefore, the inclusion of the multiple scattering in the simulations was found to be essential to reproduce phase and amplitude of the spectra with the correct type of atom at the right distance. In our final simulation, we refined a combination of a unit (occupancy 2, 4 coordinating oxygens) representing a bidentate acac (Scheme 5, a) and another unit (occupancy 2, 2 coordinating oxygens) representing a more remote monodentate acac (Scheme 5, b). The result of the refinement is shown in Figure 2a, with the parameters in Table 1. The agreement with the crystallographic average is good (<0.03 Å deviation for the coordinating oxygens) for the bidentate acac, whereas the distance of the monodentate ligand appears to be underestimated.

We also attempted to include the Ni-Ni interaction (average 2.869 Å in the crystal structure)[4] in our simulations but it did not improve the agreement between theory and experiment as well as the inclusion monodentate acac ligand, and did not lower the fit index significantly, and therefore we omitted it in our final simulation. As the contributions of C and Ni differ in amplitude and amplitude envelope, but not in phase, it would have been easy to mistake the contribution of the acac carbons at 2.9 Å for a Ni contribution. The similarity of the phase of C and Ni contributions leads to a large correlation between the parameters for C and Ni shells when both are included in the refinement at a similar distance; this means that the inclusion of Ni will be compensated by changes in the contribution of the C at the same distance, without a genuine improvement in the quality of the simulation. The apparent absence of a Ni-Ni contribution is the more remarkable as an EXAFS study[25] on the activation of $Ni(acac)_2$ for propene dimerization catalysis by an aluminium reagent clearly revealed the presence of the much smaller Al atom at a comparable distance; such a strong metal backscatterer is clearly absent from our spectra, however, and the observation of carbon atoms of the acac ligand that are even further away, viz. at approx. 4 Å, supports our assignment of the peaks in 3 Å region to the carbon atoms of the ligand, and not to Ni. Presumably the large static disorder in the Ni-O contribution leads to an even larger static disorder in the non-detectable Ni-Ni contribution, as this is not based on a direct bond. In an additional experiment, we tried to reduce the thermal contribution to the Debye-Waller-type factor as much as possible by measuring at 77 K, but this did not change the situation with regard to the possibility to detect the Ni-Ni contribution (Table 1, spectra not shown). This result supports an explanation in terms of static, not thermal disorder.

- - - FIGURE 1, 2, TABLE 1- - -

The EXAFS of **1b** could be simulated (Figure 2b) with just 2 bidentate acac ligands at 1.83 Å. There is no crystal structure available for this compound but the ligand geometry is in good agreement with that reported in a crystallographic study of a $Ni(acac)_2$ complex in which the acac methyl groups are replaced by t-butyl groups;[16] this is square-planar with 4 Ni-O bonds with an average bond length of 1.83 Å.

The X-ray absorption edge (XANES) spectra of the $Ni(acacR)_2$ (Figure 3) also reflect the large change in Ni coordination sphere that results from the introduction of the bulky substituent in going from **1a** to **1b**. There is also in some of the spectra a small shift to higher energy which points to a subtle decrease in average ligand distance;[26] this is consistent with some contraction of the material, including the metal-ligand distances, at lower temperature. As we expected to be able to use this part of the spectrum to detect subtle redox effects, i.e. oxidation or reduction of the Ni(II) ion, upon introduction of reactants such as i-butyraldehyde and oxygen, we decided to try to understand the XANES in more detail. Following our discovery, in our work on Ni-isocyanide complexes,[27] that the DUBBLE EXAFS station in Grenoble has a higher energy resolution we remeasured the most important samples there (Figure 4). The energy resolution at the DUBBLE EXAFS station is estimated at 1.4 eV; for the SRS a value between 1 and 3 eV is quoted depending on the energy,[15] and from our results it is estimated to be higher than 2 eV at the Ni K edge. The difference is most likely due to the higher flux at the ERSF which allows a more favourable balance between beam intensity and energy resolution.

- - - FIGURE 3, 4 - - -

Fig. 4 confirms that the Ni K-edge XANES spectra of **1a** and **1b** differ significantly, showing that XANES spectroscopy is sensitive enough to be used for the analysis of local atomic structure of nickel compounds. As mentioned in the discussion of the EXAFS simulations, there are two x-ray diffraction studies of $Ni(acac)_2$ (**1a**), giving the crystallographic structure of this compound.[3,4] We have made theoretical simulations of Ni K-edge XANES using Ni and O coordinates from both sets of data (Fig. 5a) and found that the spectrum obtained using the structure from Ref. 4 is in better agreement with experimental curve (see Fig. 5b). Thus, one can conclude that the more recently

obtained crystallographic results[4] are a better representation of the real structure of **1a**. It is remarkable that the XANES can be reproduced by a 3-dimensional structure of Ni and O atoms without the ligand C atoms, the more so as the C atoms were preferred to the Ni atoms in the EXAFS simulations (see above); one should note, however, that the XANES is less sensitive to static disorder, as no 'Debye-Waller-type' factor is used in the simulations.

- - - FIGURE 5 - - -

Because the substituted analogue **1b** has not been studied by XRD there is no existing structural model for this compound. Based on the EXAFS results, in which the bidentate acac moieties were treated independently and intra-ligand effects were not taken into account, it is possible that this complex is square-planar, as is possible for this type of complex (see crystal structure of an analogue[16] and Fig. 6a, top), or that one of its two acac moieties is rotated by 90° with respect to the other, leading to a tetrahedral arrangement for the coordinating oxygen atoms (Fig. 6a, bottom). We have used the coordinates of the neighbouring atoms around Ni ion site obtained in the present study from EXAFS analysis to simulate the XANES spectrum. As one can see from Fig. 6b the spectrum of the "rotated" molecule differs much more significantly from the experimental curve than the spectrum of the "planar" molecule: there is no D shoulder and the energy position of minimum D' is shifted. Therefore one can conclude that the square-planar structure of substituted $Ni(acac)_2$ (Fig. 6a, top) is favoured over the tetrahedral one (Fig. 6a, bottom).

- - - FIGURE 6 - - -

EXAFS of Ni(acacR)$_2$ in solution with and without coreactant. In Figure 7 (left), a comparison is made between the Ni environment in $Ni(acac)_2$ (**1a**) in the solid state, and in toluene solution in the absence and presence of the coreactant, i-butyraldehyde. Non-substituted **1a** appears to retain its trimeric structure upon dissolution in toluene; there is a slight decrease in EXAFS amplitude which could indicate some dissociation. Upon addition of isobutyraldehyde, the full amplitude for 6-coordinated Ni is restored. The simplest explanation for these observations is that i-butyraldehyde binding proceeds by a mechanism as shown in the top right half of Scheme 6, i.e. dissociation of the trimer, followed by association of the monomer with i-butyraldehyde to give again 6-coordinated Ni. However, in view of the fact that the Ni-Ni interactions are not detected by EXAFS in

this system, it is still possible that the complexes with i-butyraldehyde are oligomeric in nature, and that the binding follows the mechanism given in the bottom left half of Scheme 6, i. e. attack of the i-butyraldehyde on the trimer, followed by gradual dissociation into dimers and monomers, depending on the i-butyraldehyde concentration. The error in our determination of the relative occupancies of acac and coreactant is too large to allow the different possibilities in the bottom half of Scheme 6 to be distinguished.

- - - FIGURE 7, SCHEME 6 - - -

Figure 7 (right) shows a comparison of the spectra of $Ni(acacR)_2$ (R = p-tBuPh, **1b**) in the solid state and in solution in the absence and presence of the i-butyraldehyde coreactant. The collapse of the major peak of **1b** upon dissolution in toluene indicates that a dynamic monomer-trimer equilibrium exists in which the Ni environment is disordered, with a lower degree of association than for **1a**. Compared to the situation for **1a**, the ligand association equilibrium depicted in Scheme 3 and 6 lies more to the monomer side for **1b**, though not as completely as for **1b** in the solid state. Excess isobutyraldehyde gives a higher occupancy and/or lower disorder of the first shell, consistent with direct coordination of this coreactant, but the complexation is not as complete as for **1a**. Both the lower degree of association and in affinity for i-butyraldehyde of **1b** compared to **1a** can be explained by the steric hindrance due to the bulky substituent in **1b**.

The XANES spectra of the solutions were virtually identical (not shown) and resembled that of solid **1a** apart from a shift of 0.5 eV to lower energy, and a reduction of the intensity of the white line by 5 %; this was not further investigated. Simulations for the EXAFS data of solutions of **1a** and **1b** are shown in Figure 8 and 9, respectively; parameters for these refined simulations are given in Table 2. In the final simulations, the solutions of the acac complexes were modeled by analogy to solid **1a**, i.e. with 2 bidentate (4 O's) and 2 monodentate (2 O's) acac ligands per Ni. In the solutions with excess i-butyraldehyde, the monodentate acac ligands were replaced by i-butyraldehyde. No attempt was made, not by varying the occupancies nor by applying fractional occupancies for the different units, to quantify the observed trends in amplitude of the EXAFS signal that was discussed above in terms of dissociation/association equilibria and varying amounts of i-butyraldehyde binding; this would have been futile in view of

the well-established inaccuracy of EXAFS in the determination of coordination numbers (estimated error: ± 20 %).

- - - FIGURE 8, 9, TABLE 2 - - -

EXAFS of polymer supported Ni(acac)$_2$. The polybenzimidazole (PBI, active)[5] and aminomethylpyridine methacrylate polymer (AMP-resin, inactive) have some effect on the Ni environment in **1a** as weak contributions of the heteroaromatic ligands (benzimidazole and pyridine, respectively) are detected at higher R in the Fourier transform (Figure 10). The XANES spectra (Figure 3) of the polymer-supported catalysts look quite similar to that of **1a**, suggesting only small changes. In a study[6] of Mo acac complexes grafted on PBI, the acac ligand was found to be completely displaced by the benzimidazole nitrogens. In view of the similarity of the spectra to that of **1a**, this is unlikely to have happened in the case of the Ni(acac)$_2$ complexes, but some displacement must have taken place; the strong contribution at 3 Å in the phase-corrected Fourier transform of the AMP-resin EXAFS is reminiscent of pyridine coordination.[28] The simulations in Fig. 11, with the parameters in Table 3, are based on a combination of 2 bidentate acac units (4 coordinating oxygens) with 2 heteroaromatic units, i.e. imidazole for PBI and pyridine for AMP-resin, and indicate that displacement of the acac ligand by the heteroaromatic ligands is significant, but also far from complete. Because of the inaccuray of EXAFS in the determination of coordination numbers, it could be that the actual fraction of heteroaromatic ligand coordination is somewhat higher or lower than used in the simulation, but it is certain that both acac and heteroaromatic ligand contribute.

- - - FIGURE 10, 11, TABLE 3 - - -

It has been found that the mixed complex of Ni with acac and pyridine crystallizes as a dimer of a structure like that in the bottom right half of Scheme 6, with pyridine instead of i-butyraldehyde;[4] such a structure cannot be entirely ruled out for the polymer-supported complex, although we do not observe the Ni-Ni contribution. The interaction with one heteroaromatic ligand, imidazole or pyridine, with the Ni(acac)$_2$ complex leads to dissociation of one acac in the monomer or oligomer, which implies that there is a vacancy in the Ni coordination sphere that is likely to interact with the i-butyraldehyde and promote catalysis. The AMP-resin which contains its pyridine ligands in flexible side chains (cf. Scheme 4) is more likely to fill such a vacancy with another ligand than the

PBI support, which has the coordinating benzimidazoles in its rigid backbone. This could be an explanation for the difference in catalytic activity[5] between the active PBI and inactive AMP-resin complexes.

Conclusions

We have shown that the 1- or 2-dimensional information derived from EXAFS can be combined with XANES to provide a 3-dimensional structure for compound **1b**, for which no single crystal X-ray diffraction structure is available. The EXAFS results for **1a** and **1b** as solid and in toluene solution show that the bulky substituent in **1b** prevents the association of monomers to trimers in the solid state, and inhibits the association equilibria in solution. The coreactant isobutyraldehyde interferes with the equilibria by coordinating to Ni in both **1a** and **1b**. The heteroaromatic ligands (benzimidazole, pyridine) in the polymeric supports PBI and AMP-resin partly displace the acac from the Ni environment; for the rigid PBI this must result in vacancies in the Ni coordination sphere, which explains why this support gives an active catalyst whereas AMP-resin does not.

Acknowledgements

The authors thank CLRC (UK) for beamtime and support (N. Chinnery, J. F. W. Mosselmans, and L. Murphy) on station 8.1 at the Daresbury Laboratory, R. de Gelder (Nijmegen) for help with crystallographic data, the EMBL Hamburg Outstation (Germany) for computing facilities, the Dutch Ministry of Economic Affairs for supporting the initial phase of this project through the IOP-Catalysis programme, and NWO (the Dutch Research Council) for providing (with FWO, the Flemish Research Council) beamtime at BM26 at DUBBLE CRG/ESRF and supporting (with RFBR, the Russian Research Council) the Dutch-Russian collaboration between Nijmegen and Rostov.

References

1. Wentzel, B. B.; Gosling, P. A.; Feiters, M. C.; Nolte, R. J. M. Kinetic Studies on the Epoxidation of Alkenes Catalyzed by Nickel(II) β-Diketonate Complexes in the Presence of Molecular Oxygen and an Aldehyde. *J. Chem. Soc., Dalton Trans.* **1998**, 2241-2246.

2. Wentzel, B. B.; Alsters, P. L.; Feiters, M. C.; Nolte, R. J. M. Mechanistic studies on the Mukaiyama epoxidation. *J. Org. Chem.* **2004**, *69*, 3453-3464.
3. Bullen, G. J.; Mason, R.; Pauling, P. The crystal and molecular structure of bis(acetylacetonato)nickel(II). *Inorg. Chem.* **1965**, *4*, 456-462.
4. Hursthouse, M. B.; Laffey, M. A.; Moore, P. T.; New, D. B.; Raithby, P. R.; Thornton, P. Crystal and molecular structures of some binuclear complexes of cobalt(II) and nickel(II) acetylacetonates with pyridines and piperidine and a refinement of the crystal and molecular structure of hexakis-(acetylacetonato)trinickel(II). *J. Chem. Soc., Dalton Trans.* **1982**, 307-312.
5. Wentzel, B. B.; Leinonen, S.-M.; Thomson, S.; Sherrington, D. C.; Feiters, M. C.; Nolte, R. J. M. Aerobic Epoxidation of Alkenes Using Polymer Bound Transition Metal β-Diketonate Complexes as Catalysts and Aldehydes as Co-reagents. *J. Chem. Soc., Perkin Trans.* **2000**, *1*, 3428-3431.
6. S. Leinonen, D. C. Sherrington, A. Sneddon, D. McLoughlin, J. Corker, C. Canevali, F. Morazzoni, J. Reedijk, S. B. D. Spratt, Molecular structural and morphological characterization of polymer-supported Mo(VI) alkene epoxidation catalysts. *J. Catal.* **1999**, *183*, 251-266.
7. Lindsay, D.; Sherrington, D. C. *Reactive Polymers* **1985**, *3*, 327-339.
8. Sprakel, V. S. I.; Feiters, M. C.; Nolte, R. J. M.; Hombergen, P. H. F. M.; Groenen, A.; de Haas, H. J. R. A cell for combined UV-visible and x-ray absorption spectroscopy studies under low-temperature and air exclusion conditions. *Rev. Scient. Instr.* **2002**, *73*, 2994-2998.
9. 'X-ray Absorption Spectroscopy' (Koningsberger, D. C.; Prins, R., editors) Wiley, New York, **1988**, pp. 257-320.
10. Gurman, S. J., Binsted, N.; Ross, I. A rapid, exact, curved-wave theory for EXAFS calculations. *J. Phys. C., Solid State Phys.* **1984**, *17*, 143-151.
11. Gurman, S. J., Binsted, N.; Ross, I. A rapid, exact, curved-wave theory for EXAFS calculations. II. The multiple scattering contributions. *J. Phys. C., Solid State Phys.* **1986**, *19*, 1845-1861.
12. Binsted, N., Strange, R. W.; Hasnain, S. S. Constrained and restrained refinement in EXAFS data analysis with curved wave theory. *Biochemistry* **1992**, *31*, 12117-12125.
13. A. Bianconi in *X-ray Absorption: Principles, Applications and Techniques of EXAFS, SEXAFS and XANES* (Eds.: D.C. Koningsberger, R. Prins) John Wiley& Sons, New York, **1989**, pp. 573-662.
14. Cramer, S. P.; Eidsness, M. K.; Pan, W.-H.; Morton, T. A.; Ragsdale, S. W.; DerVartanian, D. V.; Ljungdahl, L. G.; Scott, R. A. X-ray absorption spectroscopic

evidence for a unique nickel site in *Clostridium thermoaceticum* carbon monoxide dehydrogenase. *Inorg. Chem.* **1987**, *26*, 2477-2479.
15. van der Hoek, M. J.; Werner, W.; van Zuylen, P.; Dobson, B. R.; Hasnain, S. S.; Worgan, J. S.; Luickx, G. A slitless double crystal monochromator for EXAFS and XANES measurements. *Nucl. Inst. and Methods* **1986**, *A246*, 380-384.
16. Cotton, F. A.; Wise, J. J. The crystal and molecular structure of bis(2,2,6,6-tetramethylheptane-3,5-dionato)nickel(II). *Inorg. Chem.* **1966**, *5*, 1200-1207.
17. Bear, C. A.; Duggan, K. A.; Freeman, H. C. Tetraimidazolezinc(II) perchlorate. *Acta Cryst. B* **1975**, *31*, 2713-2715.
18. Beurskens, G.; Martens, C. F.; Nolte, R. J. M.; Beurskens, P. T.; Smits, J. M. M. Crystal and molecular structure of tetrapyridyl-copper(II)-bis-nitrato-bis-pyridine. *J. Chem. Crystal.* **1995**, *25*, 425-427.
19. Ankudinov, A. L.; Bouldin, C. E.; Rehr, J. J.; Sims, J.; Hung, H. Parallel calculation of electron multiple scattering using Lanczos algorithms. *Phys. Rev. B.* **2002**, *65*, 104107-104117.
20. Benfatto, M.; Congiu-Castellano, A.; Daniele, A.; Della Longa, S. MXAN: a new software procedure to perform geometrical fitting of experimental XANES spectra. *J. Synchrotron Rad.* **2001**, *8*, 267-269.
21. Della Longa, S.; Pin, S.; Cortes, R.; Soldatov, A.; Alpert, B. Fe-heme conformations in ferric myoglobin. *Biophys J.* **1998**, *75*, 3154-3162.
22. Yalovega, G.; Soldatov, A. V.; Riedler, M.; Pederson, M. R.; Kolmakov, A.; Novak, C.; Mőller, T. Geometric structure of $(NaCl)_4$ clusters studied with XANES at the chlorine L-edge and at the sodium K-edge. *Chem. Phys. Lett.* **2002,** *356*, *23-28.*
23. Joly, Y. X-ray absorption near-edge structure beyond the muffin-tin approximation. Y. *Phys. Rev. B.* **2001**, *62*, 125120.
24. Joly, Y. Calculating X-ray absorption near-edge structure at very low energy. *J. Synchr. Rad.* **2003**, *10*, 58-63.
25. Corker, J. M.; Evans, J. EXAFS studies of the activation of homogenous nickel catalysts for propene dimerisation by aluminum reagents. *J. Chem. Soc., Chem. Commun.* **1991**, 1104-1106.
26. Dau, H., Liebisch, P. & Haumann, M. X-ray absorption spectroscopy to analyse nuclear geometry and electronic structure of biological metal centers – potential and questions examined with special focus on the tetra-nuclear manganese complex of oxygenic photosynthesis. *Anal. Bioanal. Chem.* **2003**, *376*, 562-583.
27. Metselaar, G. A.; Nikitenko, S.; Feiters, M. C. manuscript in preparation

28. Feiters, M. C.; Klein Gebbink, R. J. M.; Solé, V. A.; Nolting, H.-F.; Karlin, K. D.; Nolte, R. J. M. X-ray absorption spectroscopic studies of the Cu(I) complexes of crown ether appended bis-{(2-pyridyl)ethyl}amines and their dioxygen adducts. *Inorg. Chem.* **1999**, *38*, 6171-6180.

Figure Captions

Scheme 1. Structure of $Ni(acacR)_2$ and example of an aerobic reaction catalyzed by it, viz. selective epoxidation of limonene, with *i*-butyraldehyde as a coreactant.

Scheme 2. Proposal for the mechanism of the $Ni(acac)_2$ catalysed aerobic Mukaiyama alkene epoxidation with an aldehyde coreactant, adapted from ref. 2.

Scheme 3. Association/dissociation of Ni acac complexes, adapted from ref. 3.

Scheme 4. Structures of PBI (polybenzimidazole) and AMP-resin supports.

Scheme 5. Geometries of ligands adapted from crystallography and used in EXAFS simulations.

Scheme 6. Proposed effect of the i-butyraldehyde coreactant on the coordination sphere and association equilibria of $Ni(acacR)_2$ complexes.

Table 1. Parameters for the simulations for Ni(acac) complexes in the solid state (Fig. 2).

Table 2. Parameters for the simulations for Ni(acac) in solution (Fig. 8, 9).

Table 3. Parameters for the simulations for Ni(acac) on support (Fig. 11).

Figure 1. EXAFS (top panels) and modulus of the phase-corrected Fourier transform (bottom panels) of $Ni(acacR)_2$, comparison of **1a** (solid) and **1b** (dashed) in solid state in BN.

Figure 2. EXAFS (top panels) and phase-corrected Fourier transform, including imaginary part (bottom panels), of $Ni(acacR)_2$, experimental (solid lines) and simulation (dotted lines); a) best simulation for **1a**; b) best simulation for **1b**; simulation parameters in Table 1.

Figure 3. Comparison of XANES measured at the SRS (Daresbury Laboratory) of (top to bottom) **1b**, **1a**, **1a** on PB, and **1a** on PBI. Solid lines, room temperature; dashed lines, 77 K.

Figure 4. The experimental Ni K-edge XANES of **1a** (solid line) and **1b** (dashed line), measured at DUBBLE/ESRF.

Figure 5a. Arrangement of the Ni (black) and O (grey) atoms used in the simulations in Figure 5b.
Figure 5b. The Ni K-edge XANES of $Ni(acac)_2$ (**1a**): experiment (solid line), theoretical simulations based on the original (ref. 3, dotted line) and more recent (ref. 4, dashed line) crystal structure.

Figure 6a. Square planar (top) and tetrahedral (bottom) arrangement of oxygen atoms in $Ni(acacR)_2$ (R = p-tBuBn, **1b**).
Figure 6b. The Ni K-edge XANES of **1b**: experiment (solid line), theoretical simulations for planar (corresponding to Fig. 6a, top; dashed line) and rotated (corresponding to Fig. 6a, bottom; dotted line) structure, see text for details.

Figure 7. Comparison of EXAFS (top panel) and modulus of the phase-corrected Fourier transform (bottom panel) of $Ni(acacR)_2$ (left, R = H, **1a**; right, R = p-tBuBn, **1b**) in BN (solid traces) and in toluene solution in the absence (dashed traces) and presence (dotted traces) of excess i-butyraldehyde coreactant.

Figure 8. EXAFS (top panels) and phase-corrected Fourier transform, including imaginary part (bottom panels), of experimental (solid lines) and simulation (dotted lines) of **1a** a) in toluene solution; b) as a) with 460 molar equivalents of i-butyraldehyde; simulation parameters in Table 2.

Figure 9. EXAFS (top panels) and phase-corrected Fourier transform, including imaginary part (bottom panels), of experimental (solid lines) and simulation (dotted lines) of **1b** a) in toluene solution; b) as a) with 460 molar equivalents of i-butyraldehyde; simulation parameters in Table 2.

Figure 10. EXAFS (top panels) and modulus of the phase-corrected Fourier transform (bottom panels) of $Ni(acacR)_2$: solid, **1a**; dashed, **1a** on PBI; dotted, **1a** on AMP-resin; thin line, **1b**.

Figure 11. EXAFS (top panels) and phase-corrected Fourier transform, including imaginary part (bottom panels), of experiment (solid line) and simulation (dotted line) of **1a** on a) PBI, and b) AMP-resin; simulation parameters in Table 3.

Table 1. Environment of Ni in **1** determined by X-ray diffraction of single crystals and by EXAFS of powders diluted with BN. EXAFS parameters derived from refined simulations: distances to Ni in Å, Debye-Waller-type factors as $2\sigma^2$ in $Å^2$ in parentheses, ΔEF (threshold energy) in eV.

	1a crystal[a)] structure	**1a** EXAFS RT	**1a** EXAFS 77 K	[b)] crystal structure	**1b** EXAFS RT	**1b** EXAFS 77 K
4 O*	1.996	2.028 (0.038)	2.018 (0.024)	1.842	1.828 (0.006)	1.829 (0.007)
4 C*	2.912	2.946 (0.019)	2.933 (0.023)	2.829	2.793 (0.010)	2.798 (0.024)
2 C*	3.250	3.238 (0.002)	3.242 (0.002)	3.213	3.280 (0.003)	3.259 (0.003)
4 C*	4.285	4.327 (0.017)	4.326 (0.015)	4.201	4.201 (0.019)	4.192 (0.035)
2 O#	2.086	2.036 (0.004)	2.051 (0.003)	-	-	-
2 C#	3.063	3.037 (0.039)	3.052 (0.037)	-	-	-
2 C#	4.168	4.181 (0.006)	4.184 (0.036)	-	-	-
1 C#	3.633	-	-	-	-	-
ΔEF	-	0.4902	0.6625	-	2.3546	3.4986
FI [c)]	-	0.2542	0.1922	-	0.5393	0.6470
		Fig. 2a			Fig. 2b	

[a)] Average values from the structure for **1a** reported in ref. 4.

[b)] Average values from the structure for bis(2,2,6,6-tetramethylheptane-3,5-dionato)nickel(II) from ref. 16.

[c)] FI, Fit index, with k^3-weighting

* bidentate acac ligand

monodentate acac ligand

Table 2. Refined parameters for the simulations of the EXAFS of solutions of **1** in toluene with and without 460 molar equivalents of *i*-butyraldehyde (iBu=O). EXAFS parameters derived from refined simulations: distances to Ni in Å, Debye-Waller-type factors as $2\sigma^2$ in $Å^2$ in parentheses, ΔEF (threshold energy) in eV.

	1a sol'n toluene	**1a** + iBu=O	**1b** sol'n toluene	**1b** + iBu=O
4 O*	2.002 (0.026)	2.044 (0.033)	2.026 (0.032)	2.032 (0.029)
4 C*	2.920 (0.017)	2.961 (0.033)	2.962 (0.030)	2.958 (0.032)
2 C*	3.201 (0.002)	3.381 (0.019)	3.234 (0.038)	3.376 (0.038)
4 C*	4.284 (0.014)	4.320 (0.004)	4.319 (0.021)	4.323 (0.006)
2 O#	2.074 (0.009)	2.047 (0.008)	2.062 (0.020)	2.066 (0.008)
2 C#	3.090 (0.002)	3.059 (0.007)	3.096 (0.008)	3.066 (0.003)
2 C#	4.205 (0.039)	4.527 (0.009)	4.191 (0.033)	4.526 (0.011)
ΔEF	0.6701	0.1053	0.1053	-0.3049
FI[a)]	0.6733	0.3138	0.5812	0.3381
	Fig. 8a	Fig. 8b	Fig. 9a	Fig. 9b

* From bidentate acac ligand

From monodentate acac ligand or (if present) coordinating *i*-butyraldehyde

a) FI, fit index with k^3-weighting

Table 3. Refined simulations for **1a** on PBI (polybenzimidazole) and AMP-resin. EXAFS parameters derived from refined simulations: distances to Ni in Å, Debye-Waller-type factors as $2\sigma^2$ in $Å^2$ in parentheses, ΔEF (threshold energy) in eV.

PBI, bidentate acac unit	PBI, imidazole acac unit	AMP-resin, bidendate acac unit	AMP-resin, pyridine unit
4 O @ 2.072 (0.020)	2 N @ 2.043 (0.017)	4 O @ 2.115 (0.010)	2 N @ 1.988 (0.004)
4 C @ 2.894 (0.028)	4 C @ 3.078 (0.012)	4 C @ 2.957 (0.009)	4 C @ 2.907 (0.020)
2 C @ 3.431 (0.020)	4 C/N @ 4.151 (0.033)	2 C @ 3.144 (0.021)	4 C @ 4.220 (0.035)
4 C @ 4.362 (0.033)		4 C @ 4.383 (0.002)	2 C @ 4.735 (0.008)
ΔEF, 3.0461 eV FI, [a] 0.2549		ΔEF, 1.6526 eV FI, [a] 0.3228	
Fig. 11a		Fig. 11b	

[a] FI, fit index with k^3-weighting

Figures

Scheme 1.

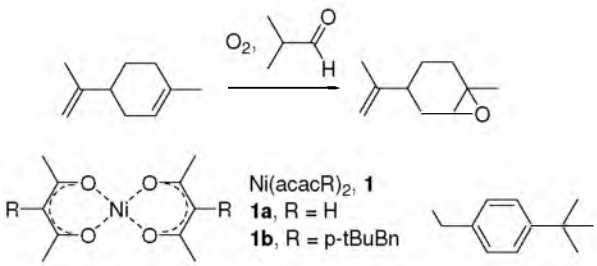

Scheme 2.

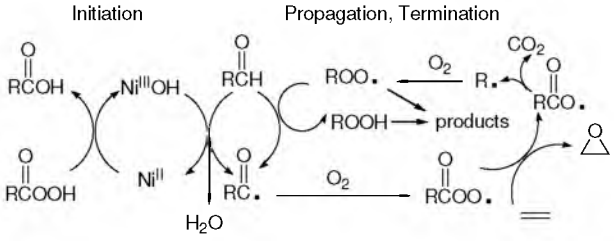
Initiation
Propagation, Termination
RCOH
Ni^III OH
RCH
ROO.
O2
R.
CO2
RCO.
ROOH
products
RCOOH
Ni^II
RC.
O2
RCOO.
H2O

Scheme 3.

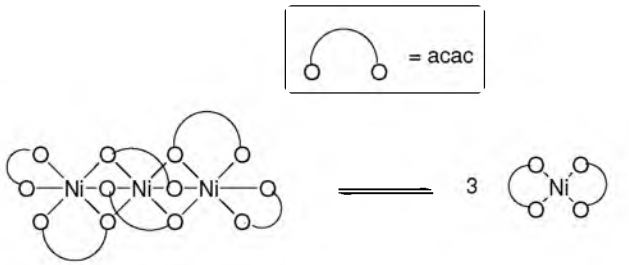

Scheme 4.

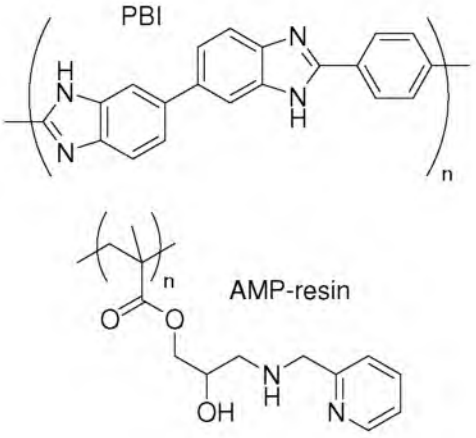

Scheme 5.

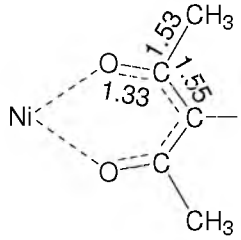

Ni-O-C 124°
Ni-O--CH_3 161°
Ni-O--C 92°

a) bidentate acac

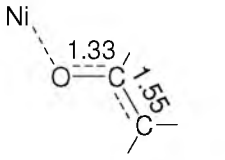

Ni-O-C 126°
O-C-C 126°
Ni-O-C-C 147°

b) bidentate acac

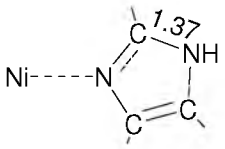

c) imidazole

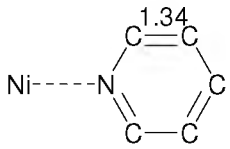

d) pyridine

Scheme 6.

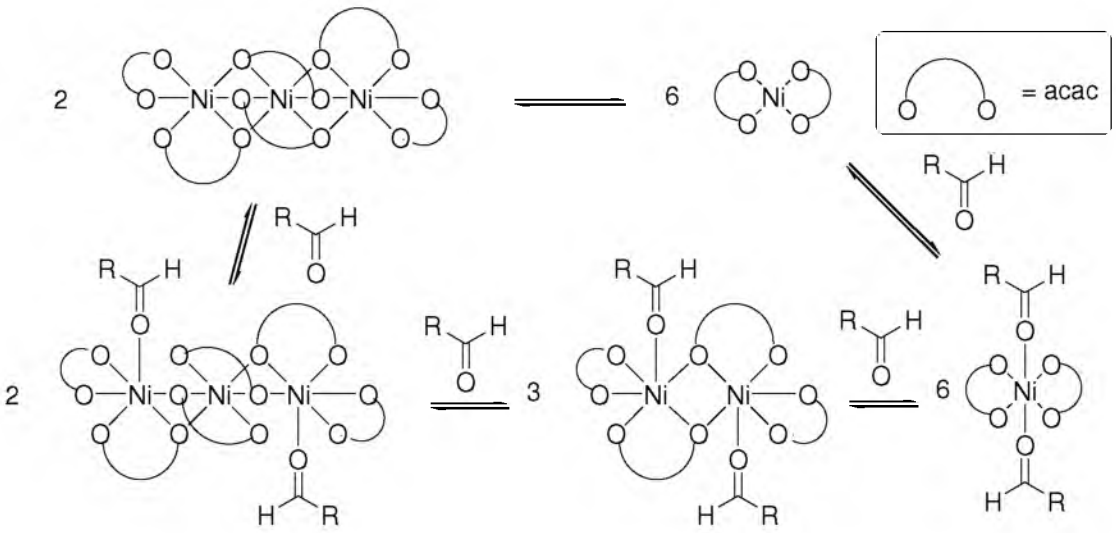

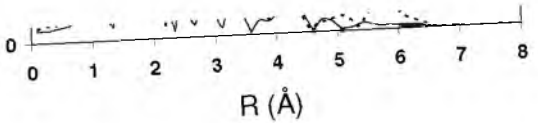
0
0 1 2 3 4 5 6 7 8
R (Å)

Figure 1.

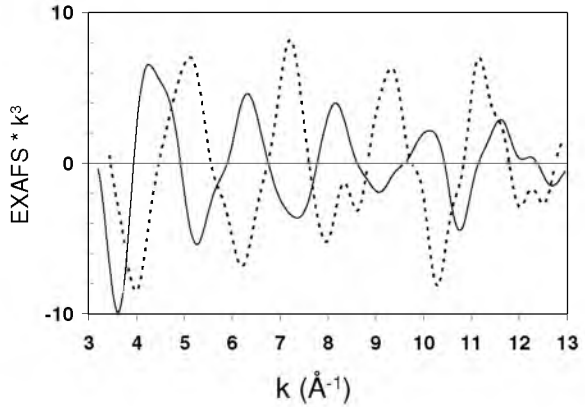

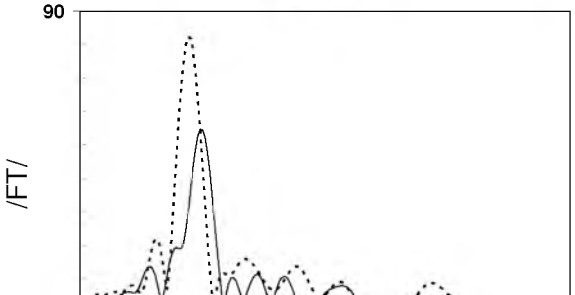

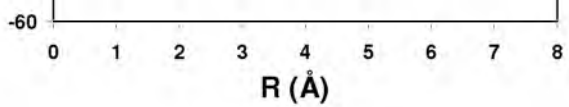
-60
0
1
2
3
4
5
6
7
8
R (Å)

Figure 2a.

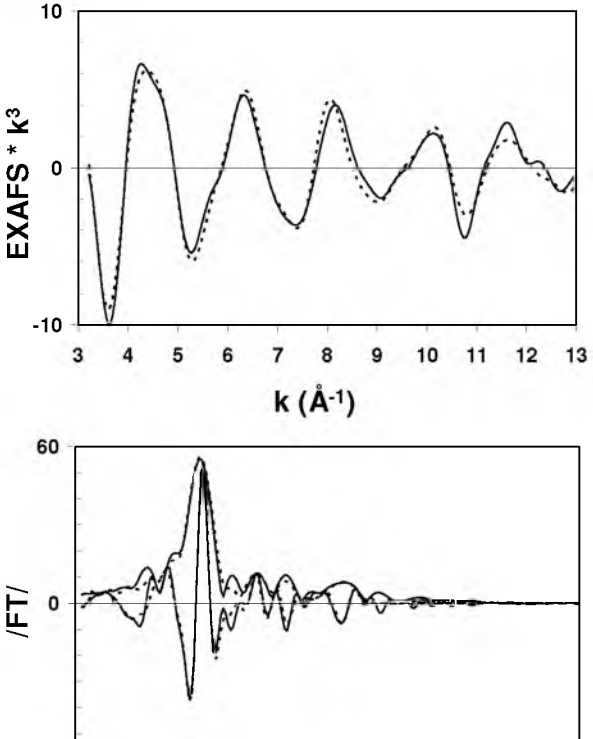

Figure 2b.

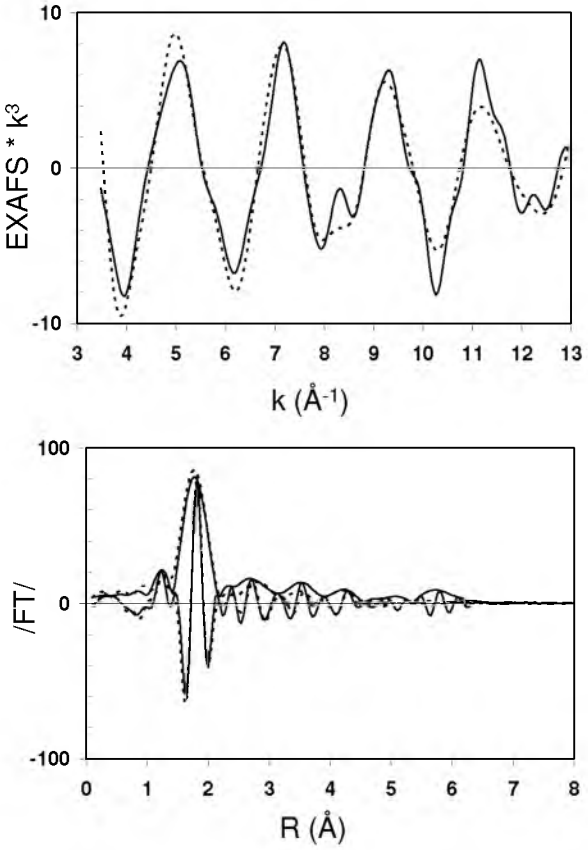
10
0
-10
EXAFS * k3
3 4 5 6 7 8 9 10 11 12 13
k (Å-1)
100
0
-100
/FT/
0 1 2 3 4 5 6 7 8
R (Å)

Figure 3.

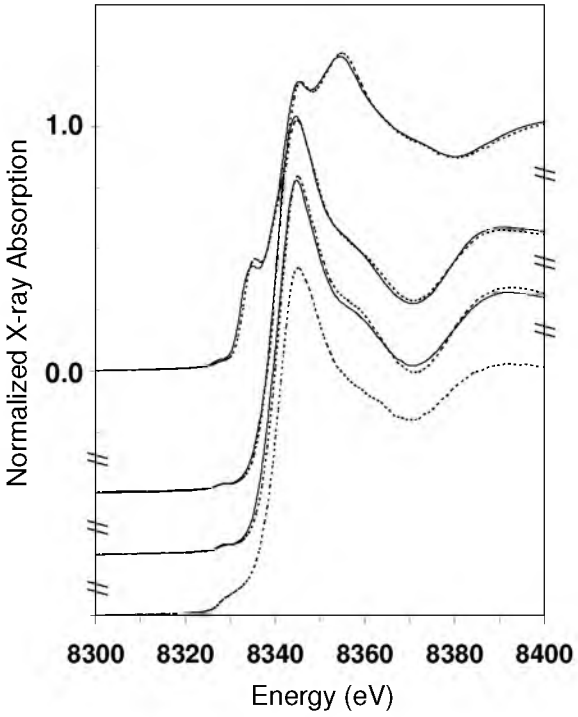
Normalized X-ray Absorption
1.0
0.0
8300
8320
8340
8360
8380
8400
Energy (eV)

Figure 4.

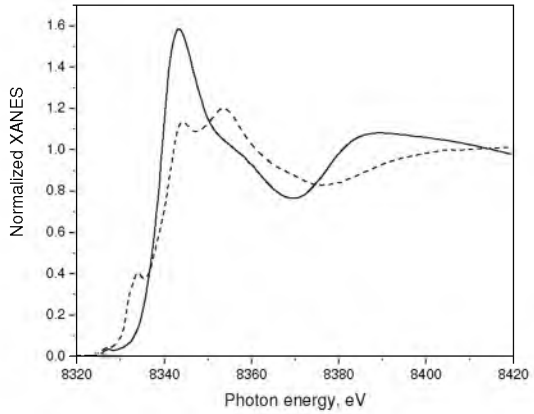
Normalized XANES
1.6
1.4
1.2
1.0
0.8
0.6
0.4
0.2
0.0
8320
8340
8360
8380
8400
8420
Photon energy, eV

Figure 5a.

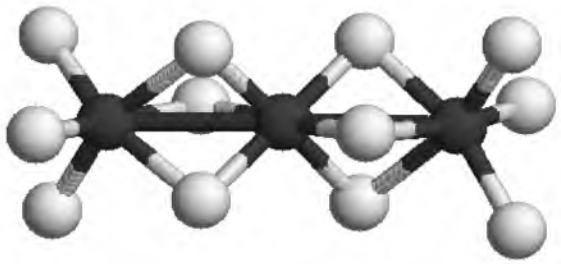

Figure 5b.

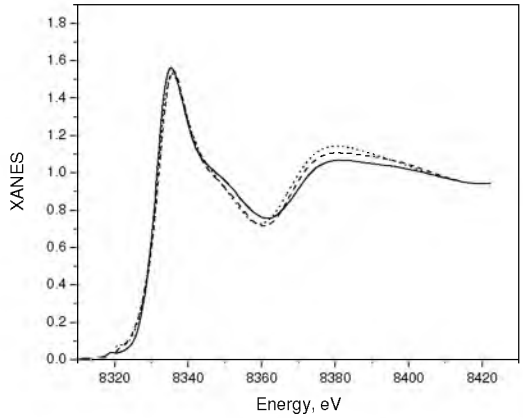
XANES
1.8
1.6
1.4
1.2
1.0
0.8
0.6
0.4
0.2
0.0
8320
8340
8360
8380
8400
8420
Energy, eV

Figure 6a.

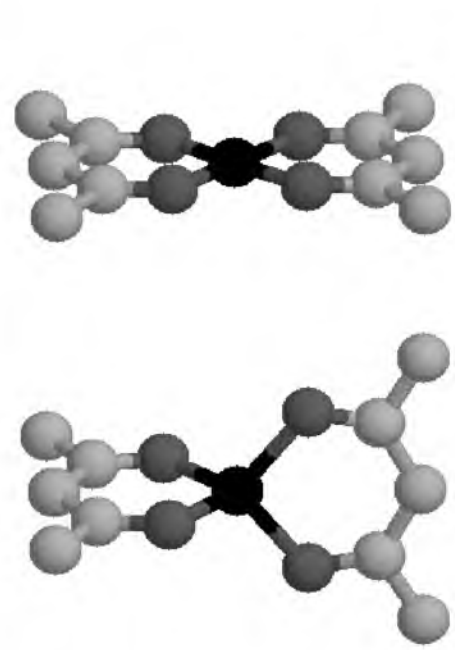

Figure 6b.

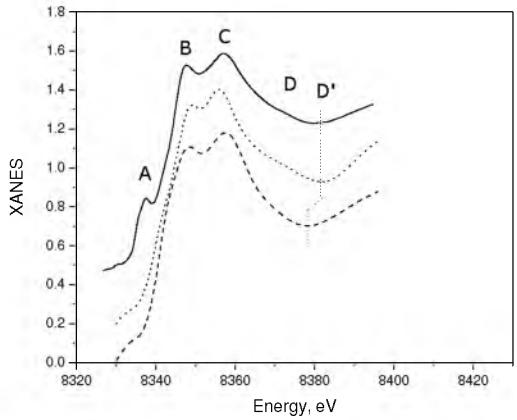
XANES
Energy, eV
A
B
C
D
D'
1.8
1.6
1.4
1.2
1.0
0.8
0.6
0.4
0.2
0.0
8320
8340
8360
8380
8400
8420

Figure 7 (left).

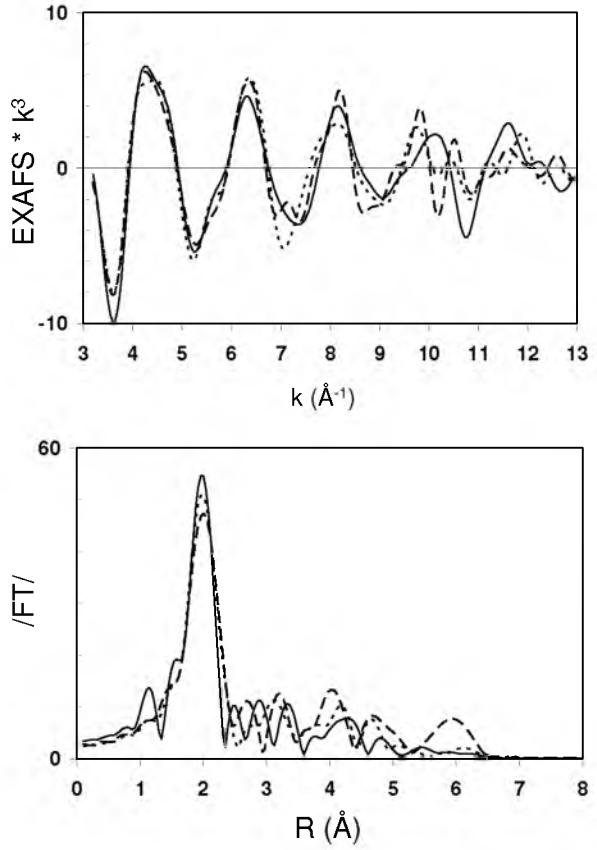

Figure 7 (right).

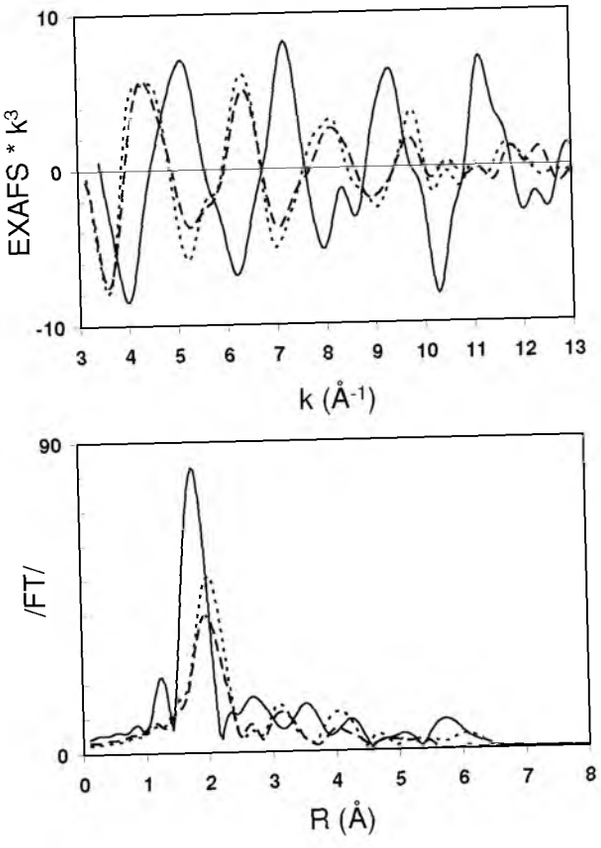

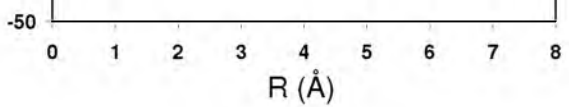
-50
0
1
2
3
4
5
6
7
8
R (Å)

Figure 8a.

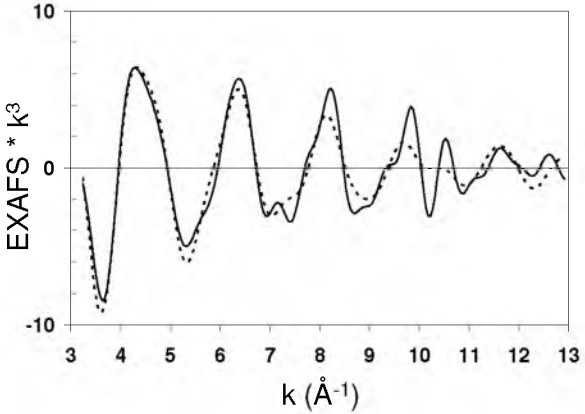

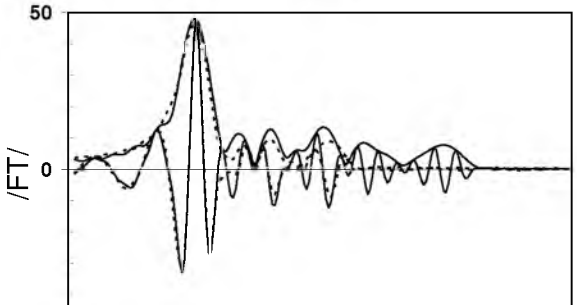

Figure 8b.

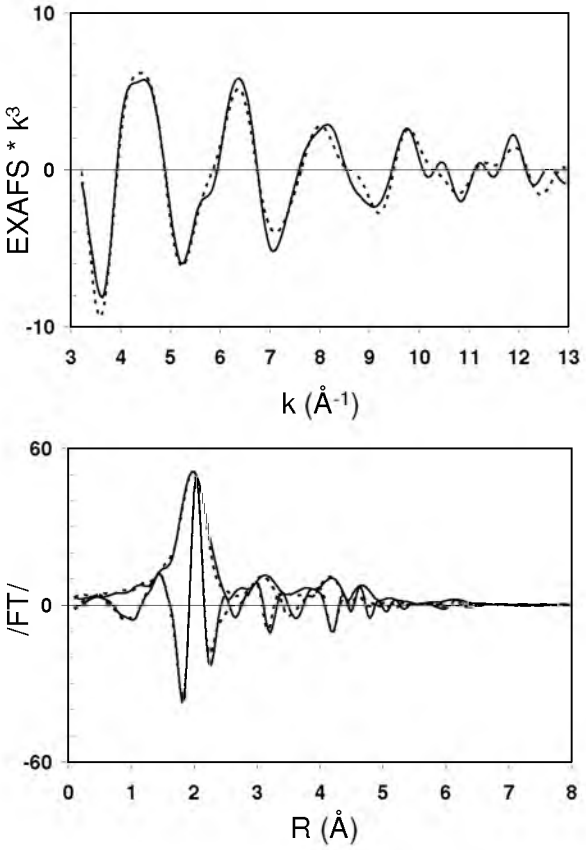

Figure 9a.

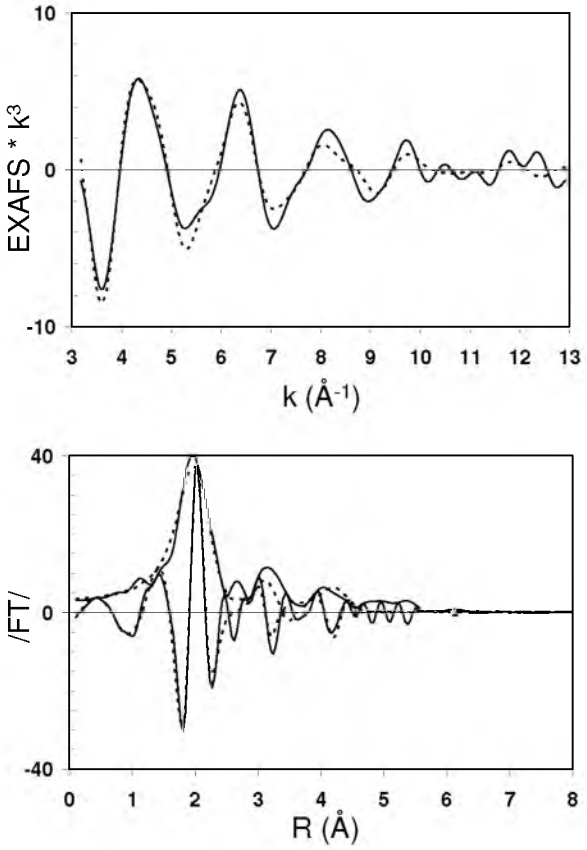

Figure 9b.

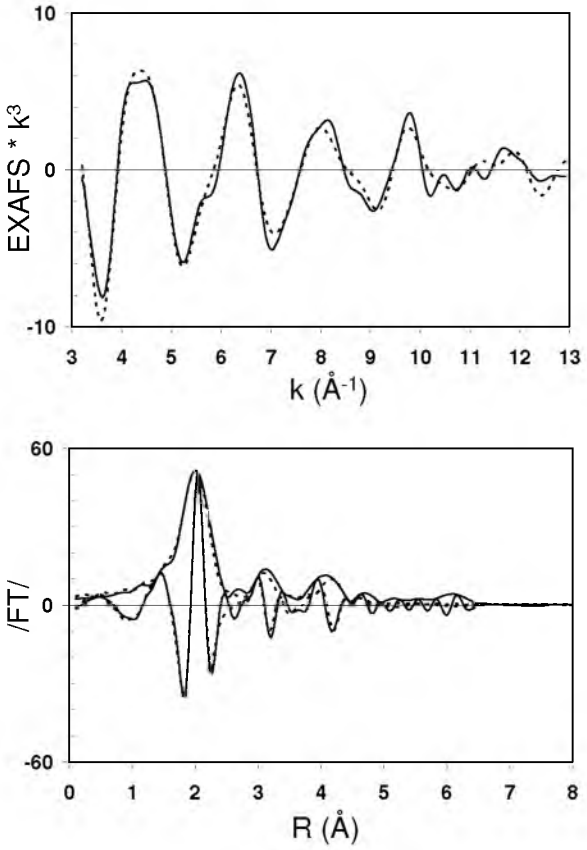

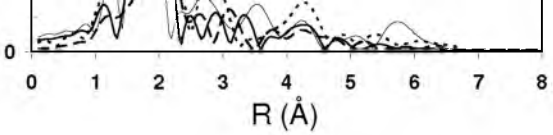
0
0
1
2
3
4
5
6
7
8
R (Å)

Figure 10.

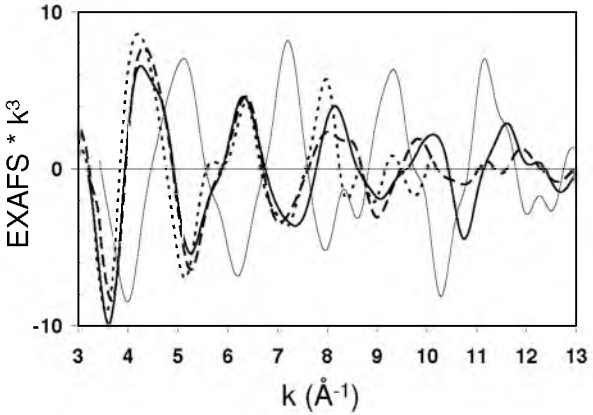

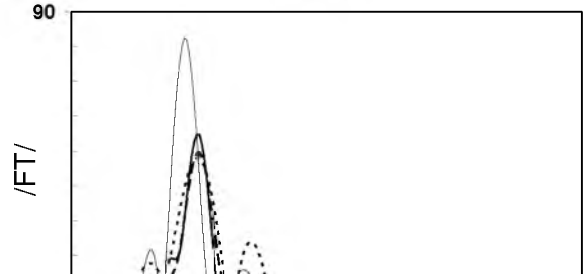

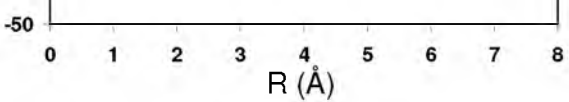
-50
0
1
2
3
4
5
6
7
8
R (Å)

Figure 11a.

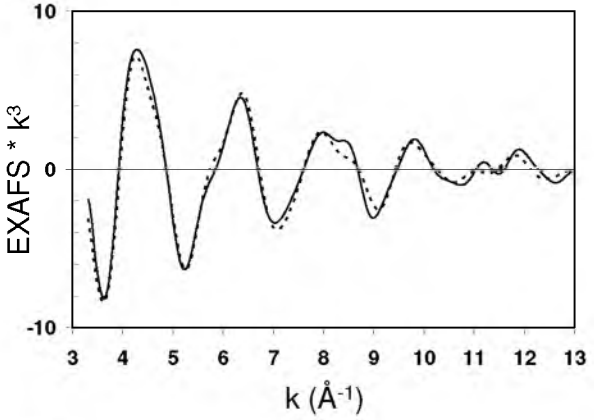

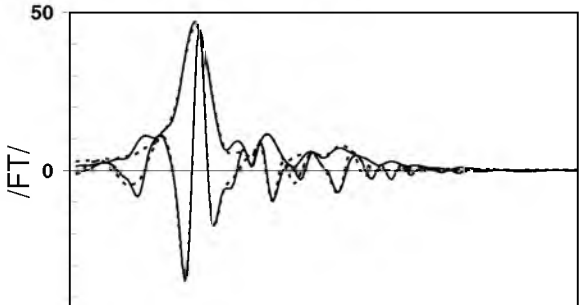

Figure 11b.